# Volumetric Fibular Transfer Planning With Shape-Based Indicators in Mandibular Reconstruction

Megumi Nakao, *Member, IEEE*, Mamoru Hosokawa, Yuichiro Imai, Nobuhiro Ueda, Toshihide Hatanaka, Tadaaki Kirita, and Tetsuya Matsuda, *Member, IEEE*

***Abstract*—In preoperative planning for mandibular reconstructive surgery, it is necessary to determine the osteotomy lines for fibular shaping and the proper placement of fibular segments in the mandible. Although virtual surgical planning has been utilized in preoperative decision making, current software designs require manual operation and a trial-and-error process to refine the reconstruction plan. We have developed volumetric fibular transfer simulation software that can quickly design a preoperative plan based on direct volume manipulation and quantitative comparison with the patient's original mandible. We propose three quantitative shape indicators—volume ratio, contour error, and maximum projection—for symmetrical lesions of the mandible, and have implemented a parallel computation algorithm for the semiautomatic placement of fibular segments. Using this virtual planning software, we conducted a retrospective study of the computed tomography data from nine patients. We found that combining direct volume manipulation with real-time local search of placement improved the applicability of the planning system to optimize mandibular reconstruction.**

***Index Terms*—Fibular transfer, mandibular reconstruction, shape indicator and volume manipulation, surgical planning.**

## I. Introduction

MICROVASCULAR free fibular transfer has become a common procedure in mandibular reconstruction [1], [2]. In this procedure, fibular segments are transplanted into the mandibular defect, conserving the curved shape and the mastication functions of the mandible [3]. The procedure includes transplanting bone segments and blood vessels from the patient's fibula to the mandible, and connecting the transferred blood vessels to those in the neck. The merits of native bone transplantation as opposed to artificial bone transplantation are quick engraftment of the bone and earlier new bone formation. The goal of this surgery is to achieve stable and precise mandibular reconstruction with structural, esthetic, and functional recovery for the patient.

In preoperative planning for mandibular reconstructive surgery, it is necessary to determine the osteotomy for fibular shaping, the number of fibular segments, and the proper placement of the fibular segments in the mandible. This planning is generally more complex than planning for artificial bone manufacture, because the patient's own fibular segments are used. Two-dimensional radiographs or CT/MRI image slices have been used in traditional preoperative planning. However, accurately segmenting and arranging the fibula according to plan are challenging even for highly skilled surgeons, and additional cutting is often needed during the operation. Although clinical efforts have been made to improve the accuracy of reconstruction [2], fibular osteotomy and mandible reconstruction remain challenging and are still largely dependent on the surgeon's experience, intraoperative decisions, and technical skills.

Virtual surgical planning has recently gained attention as a means of supporting the preoperative design of reconstructive procedures using patients' CT volume data [4]–[8]. The advantage of computer-aided planning is that it allows rapid design of a patient-specific surgical procedure, and visualization of 3-D structures that can be intuitively shared among surgeons, technicians, and other medical personnel [4]. Various reconstruction plans can be discussed using the image of the patient's own fibula superimposed onto the mandibular defect. In a recent study, a complex reconstruction called a double-barrel vascularized fibula flap was investigated, based on geometrical analysis with virtual planning software [9]. Another advantage of virtual planning is that the planned results are directly available for real stereolithographic model generation using 3-D printer systems [10], [11]. With the planning data, fibular cutting guides and a plate-bending template can be manufactured, in addition to stereolithographic models of the mandible [12], [13].

Optimizing the preoperative virtual plan is essential to improve surgical outcomes while reducing intraoperative challenges. Recent clinical studies have focused on the accuracy of virtual planning by comparing the plan with the reconstruction results [14]–[16]. Fibular segments, prefabricated surgical plates, and cutting guides planned with software were

Manuscript received March 10, 2014; revised April 17, 2014; accepted April 24, 2014. Date of publication April 29, 2014; date of current version March 2, 2015. This work was supported by the Grant-in-Aid for Scientific Research for Young Scientists (A) (21680044) from The Ministry of Education, Culture, Sports, Science and Technology, Japan.

M. Nakao and T. Matsuda are with the Kyoto University, Kyoto 606-8501, Japan (e-mail: megumi@i.kyoto-u.ac.jp; tetsu@i.kyoto-u.ac.jp).

M. Hosokawa was with the Kyoto University, Kyoto 606-8501, Japan. He is now with the NTT West, Japan (e-mail: mhosokawa@sys.i.kyoto-u.ac.jp).

Y. Imai, N. Ueda, T. Hatanaka, and T. Kirita are with the Nara Medical University, Nara 634-8521, Japan (e-mail: yimai@nmu-gw.naramed-u.ac.jp; n-ueda@naramed-u.ac.jp; thatanak@naramed-u.ac.jp; tkirita@naramed-u.ac.jp).

Color versions of one or more of the figures in this paper are available online at http://ieeexplore.ieee.org.

Digital Object Identifier 10.1109/JBHI.2014.2320720

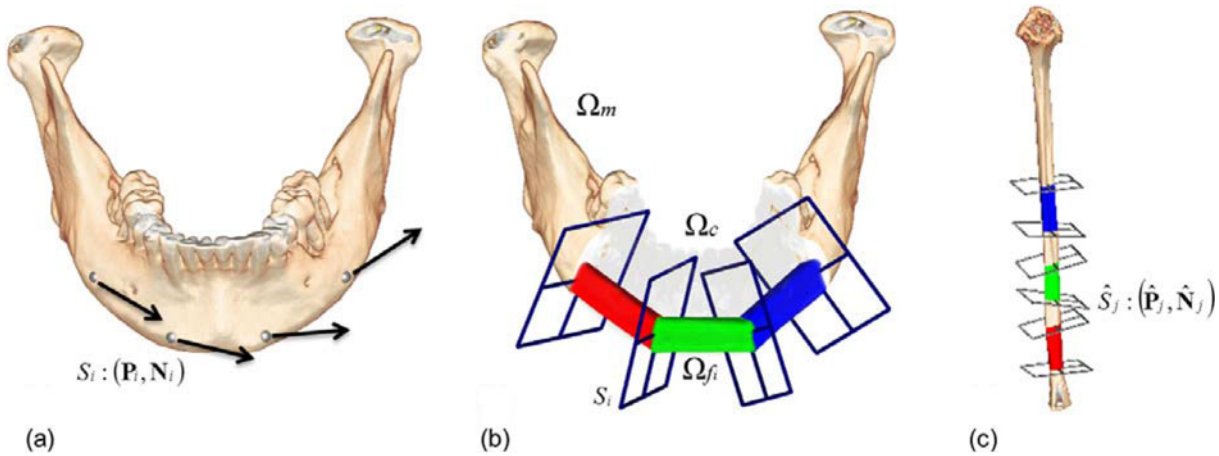


Fig. 1. Geometrical descriptions for fibular transfer simulation. (a) Initial setup of controllable virtual surfaces placed on the volumetrically rendered mandibular image, (b) three fibular segments superimposed on the resection area, and (c) original fibular volume annotated with the surgical plan. The user can interactively refine the surgical plan while observing the simulation results. The obtained cutting line is directly available for fibular osteotomy.

compared with actual treatment results. Some researchers report that the use of both virtual planning and stereolithographic models gives reliable surgical outcomes, especially in complicated cases [15], [16]. To optimize the procedure, the virtual plan should be quantitatively assessed during preoperative planning. Biomechanical behavior of the mandible after marginal resection has also been investigated based on finite-element analysis [17]. In mandibular reconstruction, the postoperative appearance of the patient's face is a key factor in improving the patient's quality of life. To address appearance, shape analysis is important, but quantitative indicators are not well established in fibular transfer surgery.

Regarding the usability of virtual planning software, current planning procedures are largely based on manual operation and require a trial-and-error process to refine the reconstruction plan [4], [11]. Because coordination and placement of fibular segments require complex procedures including 3-D translation and rotation in the virtual space, it is often difficult to achieve fine adjustment of the transfer plans, such as bone-to-bone contact. In addition, most planning software in plastic surgery uses surface representation to visualize bone structures. In fibular transfer planning, a remeshing process can occur at every step, modifying the surgical plan and shaping the fibular models. Frequent updating of the complex geometrical models is computationally cumbersome and limits the usability of the planning software. For these reasons, the use of virtual planning is currently limited to biomedical engineers, and requires additional communication between surgeons and engineers [11].

We focused on designing virtual planning software that can quickly evaluate the preoperative plan based on a quantitative comparison with the patient's original mandible. To support fibular transfer surgery, it is important to determine a mathematically adequate osteotomy and the optimal placement of the fibular segments during the mandibular reconstruction process. Much effort has been made to develop a variety of surgical planning software programs for implant surgery [18], [19], aesthetic plastic surgery [20], [21], and other orthopedic surgery [22]. To the best of our knowledge, a virtual planning system with quantitative shape indicators has not been previously described for fibular transfer surgery. In developing our program, we focused on interactive software design and user-friendly interfaces suitable for direct use by surgeons.

This paper proposes a volumetric surgical planning system that supports preoperative planning of free fibular transfer in mandibular reconstruction. Unlike previous planning software and systems, we utilize solely the volumetric representation of bone structures. This enables us to avoid the mesh generation process frequently used in shape editing. In the system we have developed, fibular segments are fused with mandibular structures and volumetrically rendered based on updates to the user's surgical plan. To optimize preoperative planning, we have introduced new shape indicators to quantify planned mandibular reconstruction for symmetrical lesions of the central part of the mandible. The proposed software and indicators were tested by applying the CT data from nine patients with oral cancer near the mentum. This paper presents some planning examples and discusses the computation results of the shape indicators.

## II. Volumetric Fibular Transfer Planning

### A. Modeling

In the proposed preoperative planning system, the resection area is first determined to ensure appropriate margins for tumor removal or for reconstruction of mandibular defects. As shown in Fig. 1, the resection area $\Omega_c$ is determined using the boundary surfaces in the mandibular image volume $\Omega_m$ and semitransparently visualized through volume rendering. We introduce a set of 3-D vectors $(\mathbf{P}_i\mathbf{N}_i)$ $(i = 0, \ldots, n, n$: the number of fibular segments) that define a virtual surface $S_i$ [see Fig. 1(a)]. $P_0$ and $\mathbf{P}_n$ represent connection points between the patient's native mandible and the fibular segments and define their boundaries [see Fig. 1(b)]. Similarly, $\mathbf{P}_k(k = 1,\ldots, n–1)$ is used as a connection point between the two fibular segments $\Omega_{f_{k-1}}$ and $\Omega_{f_k}$ .These connection points are first placed on the surface of the volumetrically rendered native mandible. When a pixel on

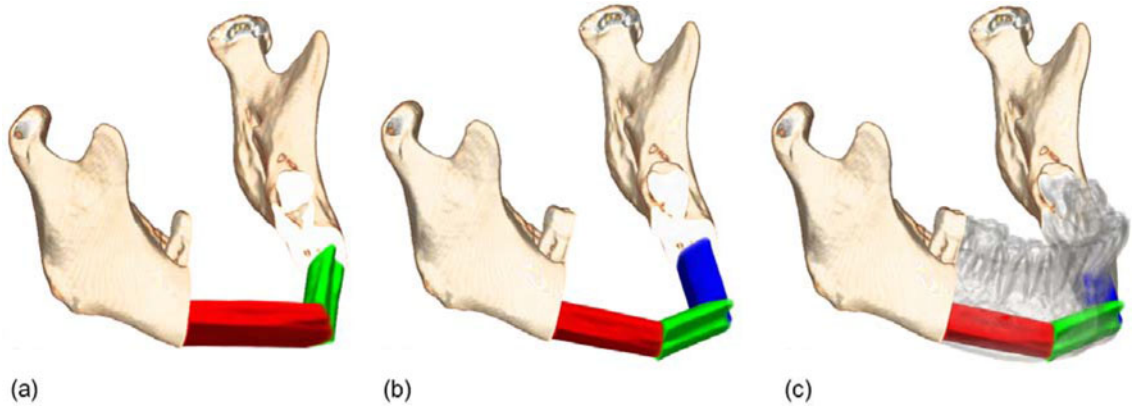


Fig. 2. Volume visualization results of fibular transfer simulation. (a) Two-segment case, (b) three-segment case, and (c) semitransparent visualization of the patient's original mandible to assess the positional relationship between teeth and fibular segments.

the rendered image is indicated, our framework estimates the corresponding voxel in the volumetric space by accumulating opacity (or alpha) values at sample points in the eye direction. This process is similar to the ray-casting protocol [23] commonly used in the volume-rendering scheme. When the accumulated opacity values exceed a threshold, we simply assume that the voxel at the current sample point was selected by the user. This direct pointing scheme in a volumetric space has also been employed in a volume sculpting study [24], [25]. Fig. 1(a) shows four connection points initially placed on the mandibular image. The position of the connection points can be modified manually or systematically. Details of the update methods are described next.

Next, another set of virtual planes $\hat{S}_j$ $(j = 0, \ldots, 2n-1)$ is configured on the fibular volume data to define fibular segments. Fig. 1(c) shows three fibular segments defined by six planes $\hat{S}_0$ , …, $\hat{S}_5$. A two-segment case is similarly defined using four virtual planes. In our system, the control point $\mathbf{P}_j$ of the virtual plane $\hat{S}_j$ is constrained on the centerline of the fibular bone. The sampled points of the centerline are precomputationally obtained through simple 2-D image processing that computes a center of gravity of the fibular area for each image slice. In addition, based on (1), each plane $\hat{S}_j$: ($\mathbf{P}_j$,$\mathbf{N}_j$) is mapped to the corresponding plane $S_i$ placed on the rendered mandibular images

$$\begin{aligned} |\mathbf{P}_{i+1} - \mathbf{P}_i| &= \left|\hat{\mathbf{P}}_{j+1} - \hat{\mathbf{P}}_j\right| \\ \mathbf{N}_{i+1} \cdot \mathbf{N}_i &= \hat{\mathbf{N}}_{j+1} \cdot \hat{\mathbf{N}}_j \qquad i = 0, \ldots, n-1, j = 2i. \end{aligned} \tag{1}$$

This scheme uniquely defines the relative positions of the virtual surfaces $\hat{S}_{2i+1}$ and $\hat{S}_{2i}$ for the fibular osteotomy, and simultaneously updates them while synchronizing with manipulation of the virtual surface $S_i$. For example, when translating or rotating the boundary surface $S_1$ between first (red) and second (green) segments, the corresponding virtual surfaces $\hat{S}_2$ and $\hat{S}_3$ are updated based on (1). Similarly, when translating or rotating the virtual surfaces $\hat{S}_2$ or $\hat{S}_3$ on the fibular image, the boundary surface $S_1$ is simultaneously updated. Thus, the user can refine the plan while observing simulation results on both the mandibular reconstruction and the fibular osteotomy.

### *B. Visualization*

The proposed simulation system has two views for visualizing the mandibular reconstruction plan. The main view renders the mandibular image with fibular transfer simulation results. Fig. 2(a) shows a planning example for mandibular reconstruction with two fibular segments. Fig. 2(b) shows another planning example using three fibular segments. The fibular segments are superimposed onto the resection area, a useful step to check visual consistency of the reconstruction plan. Contact between fibular segments and between the patient's original mandible and a fibular segment must be checked for accurate mandibular reconstruction. A fused image with cross-sectional views of the objects is important for this purpose. The second view displays the fibula with cutting lines [see Fig. 1(c)], based on the virtual surfaces configured in the main view. The estimated fibular segments are visualized by coloring part of the fibular volume. The annotated cutting lines delineate the fibular osteotomy and can be used for intraoperative support.

A key feature of this system is that it employs volume rendering to render the simulation results for all views. The surfaces of the fibular segments and of the partially resected mandibular structure are not modeled during planning. As mentioned earlier, frequent updating of the complex geometrical models can occur when modifying the surgical plan. Therefore, we do not handle 3-D shapes but we visualize transfer simulation results using volume clipping and multicolored volume rendering, which generates fused images in real time. This scheme avoids a computationally heavy modeling process and achieves interactivity. We applied a slice-based (or texture-based) volume rendering approach [26], [27] and extended it for visualization purposes.

Fig. 3 shows the basic concept of the visualization algorithm. In our system, we assume that the fibular segment $\Omega_{f_i}$ is defined by two virtual surfaces $S_i$ and $S_{i+1}$. Similarly, the resection area $\Omega_c$ is a part of the mandibular volume $\Omega_m$ between $S_i$ and $S_{i+1}$. Traditional slice-based volume rendering generates axis-aligned or view-aligned proxy planes to allow slice-by-slice sampling of the target area. In the three-segment case, four objects (i.e., the mandible and three segments) must be rendered as a fused

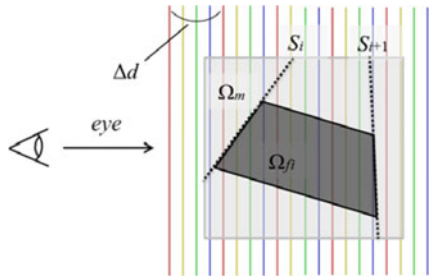


Fig. 3. Volume visualization scheme for superimpoing fibular segments on the mandibular volume. Multiple proxy planes generated from the fibular segments $\Omega_{f_k}$ and from the mandiblar volume $\Omega_m$ are fused in the eye direction and rendered from back to front.

image while keeping their depth cues. We generate a set of proxy planes from one rendering target. For example, in Fig. 3, red proxy planes are generated from the mandibular domain $\Omega_m$. The sampling pitch is $\Delta d$, and the normal vectors of the plane are parallel to the eye vector. Yellow planes with the same sampling pitch $\Delta d$ are generated from a fibular segment domain $\Omega_{f_i}$ and inserted into the space between red planes. In the same fashion, all sets of proxy planes are generated and sorted in the eye direction. Finally, the proxy planes are clipped by the given virtual surfaces and rendered from back to front using different color lookup tables.

Fig. 2(c) shows semitransparent visualization of the patient's original mandible with the superimposed fibular segments. Direct volume rendering of the internal structures allows evaluation of the positional relationship between the teeth and estimated fibular segments.

### C. Interface and Planning Procedures

In our system, all operations for preoperative planning can be performed using a 2-D pointing interface such as a standard mouse or a touch screen. This section summarizes the planning flow and the interface implemented with the developed system.

*Step 1:* (*Virtual resection*) Using the direct pointing scheme introduced earlier, the user can place the connection points $\mathbf{P}_i$ by a simple pointing operation on the rendered mandibular image. There are three connection points in two-segment cases and four in three-segment cases. Next, the resection area $\Omega_c$ and the virtual surfaces $S_i$ and $\hat{S}_j$ are initialized as a background process. The initial simulation results and the shape indicators are displayed.

*Step 2:* (*Fibular transfer simulation*) Next, the user can interactively manipulate (i.e., translate and rotate) the placed virtual planes $S_i$ and $\hat{S}_j$ to refine the surgical plan. To allow 3-D translation of the virtual surfaces, the 2-D displacement obtained by dragging the mouse is transformed into 3-D displacement $\mathbf{T_i}$ parallel to the view-aligned slicing plane. By rotating the scene, the user can interactively translate the segments in 3-D. In the case of 3-D rotation $\mathbf{R}_i$, 2-D displacement is transformed into a rotation axis and a magnitude of the angle. In response to the user's operation in one virtual plane, other virtual planes are updated simultaneously to maintain their connection and physical constraints. These operations can be interactively performed on the mandibular image with fibular segments placed in the resection area.

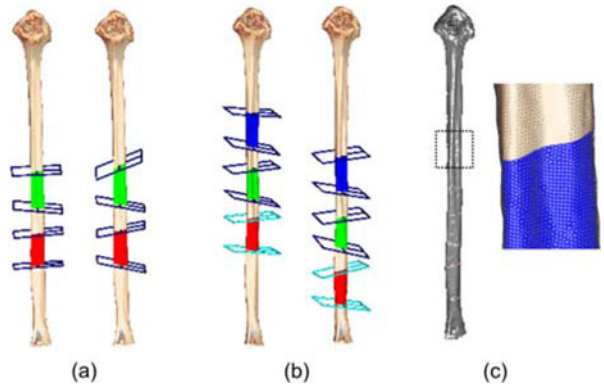


Fig. 4. Visualization and editing of the fibular segments. (a) Changes in the virtual surfaces from the initial plan, (b) selection of a thicker region, and (c) 3-D surface model annotated with the surgical plan for fibular osteotomy.

Fig. 4(a) shows the changes in the virtual surfaces between the initial placement and the planned result in a two-segment case. The user can also change segmentation of the fibular bone on the subview. A thicker portion of fibula is more appropriate for mandibular reconstruction while maintaining adequate margins for each segment [see Fig. 4(b)].

*Step 3:* (*Stereolithographic model generation*) After the reconstruction plan is formulated, the 3-D surface of the fibular bone with an annotated surgical plan [see Fig. 4(c)] is constructed for stereolithographic model production. The created model is stored in STL format and can be directly applied to a 3-D printer.

## III. Shape Indicators

To refine the reconstruction plan, traditional planning software requires trial-and-error manual operation that relies on the user's clinical experience and anatomical knowledge. Because 3-D manipulation is necessary to ascertain the optimal reconstruction plan, manual operation may cause placement errors resulting from lack of 3-D information about occlusion and depth cues, for example. To address these problems, our system implements quantitative indicators to evaluate the current planning state. As a first approach to quantification, we introduce here three shape indicators: *volume ratio*, *contour error*, and *maximum projection*.

To compute the indicators from the patient's CT data, we introduce the occlusal coordinate, a patient-specific coordinate based on the occlusal surface. In maxillofacial surgery, the occlusal surface is commonly used as an anatomical reference in restoring the mandible and its mastication function. Fig. 5(a) shows the definition of the occlusal coordinates. The three vertices are placed on the occlusal surfaces of the left and right first molars and the central incisors. The direct pointing scheme described in Section II is used to determine the 3-D position. Based on this occlusal coordinate, our system computes the following three indicators in real time.

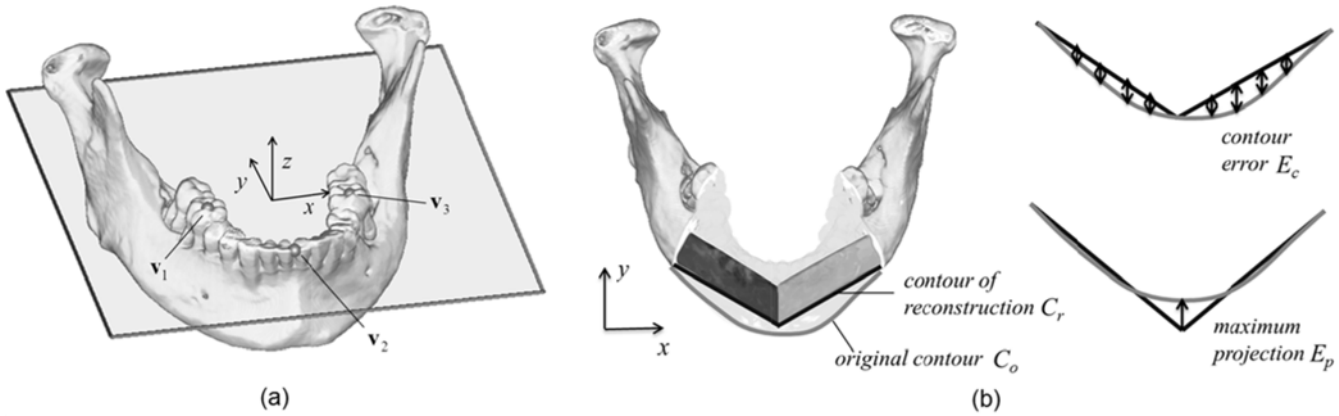


Fig. 5. (a) Three-dimensional occlusal coordinates and (b) 2-D illustration of the shape indicators to quantify geometrical differences between patient's original mandible and the reconstruction plan.

### A. Volume Ratio

The reconstructed mandible must have sufficient volume to maintain its postoperative mastication function and physical strength as a part of facial bone structure [17]. We focus especially on the volume ratio that quantifies the amount of filling of the resection regions with the fibular segments. The indicator $E_v$ for the volume ratio is described by

$$E_v = \frac{\sum V_{\mathrm{fib}}}{V_{\mathrm{cut}}} \tag{2}$$

where $V_{\mathrm{cut}}$ is the volume of the resected area and $\sum V_{\mathrm{fib}}$ is the sum of the volumes of the fibular segments placed in the resection area. This indicator is affected by fibular osteotomy and placement of the fibular segments. For example, if thicker sections are selected from the fibular volume, the indicator shows higher values.

### B. Contour Error

The postoperative appearance of the patient's face is affected by the contour of the reconstructed mandible. To quantify the contour in the given surgical plan, we define the contour error $E_c$ using the average distance between the contour of the placed fibular segments $(C_r)$ and the original contour of the patient's mandible $(C_o)$. This indicator is defined using

$$E_c = \frac{1}{n}\sum_{i=0}^{n-1} |D_r(\mathbf{p}_i) - D_o(\mathbf{p}_i)| \tag{3}$$

where $\mathbf{p}_i$ is a discrete point on the centerline of the fibula, and $n$ is the total number of discrete points. $D_o(\mathrm{p})_i$ is the scalar distance between $\mathbf{p}_i$ and the corresponding sample point on the patient's original contour $C_o$. In this computation, the *xyz*-coordinates are first placed on mandibular images based on the occlusion plane of the patient's mandible. The normal vector of the occlusal surface is set as the $z$-axis, as shown in Fig. 5(a). Next, we compute $|D_r(\mathbf{p}_i) - D_o(\mathbf{p}_i)|$ as the Euclidean distance between discrete sample points on the two contours $C_r$ and $C_o$ [see Fig. 5(b)]. The sample points are obtained by scanning two surface positions of the mandible and of the fibular segment in the $y$- and $z$-directions from the discrete points $\mathbf{p}_i$ $(i = 0, \ldots, n-1)$ composing the centerline of the fibula (see Fig. 6).

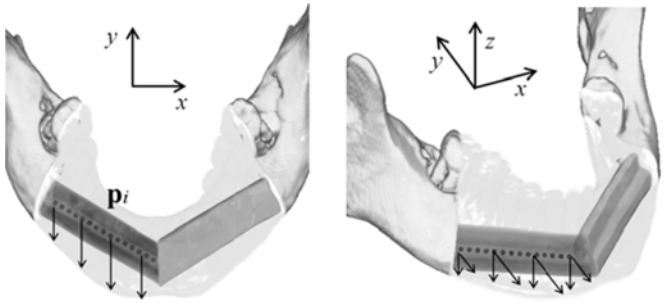


Fig. 6. Computing methods for contour error $E_c$. The surfaces of the native mandible and the fibular segment are scanned from the centerline of the fibular bone.

### C. Maximum Projection

The two shape indicators introduced earlier do not evaluate the degree to which fibular segments extend beyond the resection area [see Fig. 5(b)]. Although protruding bone can be additionally resected during surgery, the available margin for resection is restricted by the thickness of the cortex. Therefore, we employ maximum projection $E_p$ as a third indicator to filter inadequate placement of the fibular segments. $E_p$ is obtained using

$$E_p = \max_i (D_r(\mathbf{p}_i) - D_o(\mathbf{p}_i)). \tag{4}$$

## IV. Experiments and Results

We implemented the overall algorithms and software interface using C++, GLSL, and CUDA on a standard PC (CPU: Intel Core i7, 2.93 GHz, memory: 8 GB) with a general-purpose graphics card (nVidia GeForce GTX580). The developed system was tested by applying CT datasets of measurements from nine patients with oral cancer near the mentum. The CT slice images were first resampled as volume data with $256^3$ voxels. The mandible was extracted from the head CT data, and the fibula from the foot CT data. This segmentation step was completed

TABLE I
COMPUTATION RESULTS OF THE THREE SHAPE INDICATORS BASED ON DATA FROM NINE PATIENTS

| Patient | 2 segments | | | 3 segments | | |
|---|---|---|---|---|---|---|
| | *Ev* [%] | *Ec* [*mm*] | *Ep* [*mm*] | *Ev* | *Ec* | *Ep* |
| 1 | 24.85 | 2.86 | +2.15 | 25.11 | 1.77 | +3.89 |
| 2 | 22.87 | 1.37 | +2.14 | 21.89 | 1.06 | +1.36 |
| 3 | 24.68 | 2.48 | +0.54 | 25.41 | 1.30 | +1.80 |
| 4 | 35.03 | 2.93 | +4.12 | 37.54 | 1.69 | +3.86 |
| 5 | 20.53 | 3.47 | +2.08 | 23.32 | 2.18 | +1.34 |
| 6 | 25.64 | 2.43 | +1.35 | 27.34 | 1.19 | +1.47 |
| 7 | 25.54 | 2.67 | +1.61 | 27.20 | 2.17 | +0.11 |
| 8 | 24.18 | 2.50 | +1.51 | 25.89 | 1.32 | +1.42 |
| 9 | 22.70 | 2.11 | +1.91 | 25.39 | 1.33 | +1.65 |

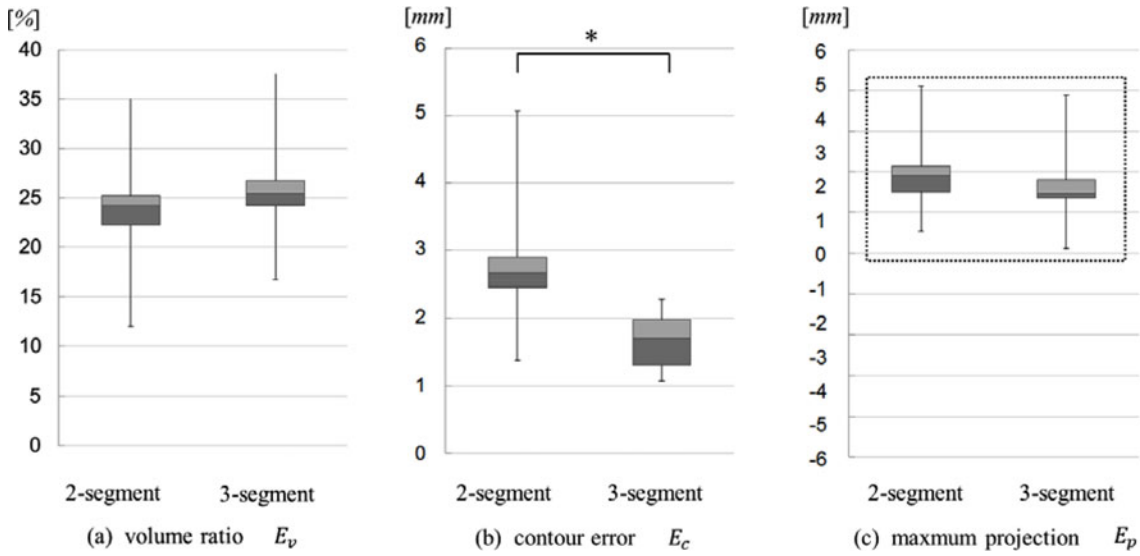


Fig. 7. Statisitical comparison of the three indicators between two-segment and three-segment cases. The contour error $E_c$ in three-segment cases is significantly lower than in two-segment cases. The maximum projection $E_p$ was a positive values in all cases.

in 2–3 min for each case, based on region growing-based ROI selection and manual removal of voxels with a 3-D cutting tool [25].

### A. Experiments

In the experiment, oral surgeons and dental technicians reproduced past surgical plans retrospectively without relying on the proposed shape indicators. Mandibular reconstruction using two and three fibular segments was interactively simulated for each patient. Fig. 2(b) shows the surgical plan adjusted through manual operation by the dental technician. Three connection points $\mathbf{P}_0, \mathbf{P}_1$, and $\mathbf{P}_2$ were first placed on the mandibular image by clicking a mouse. $\mathbf{P}_0$ and $\mathbf{P}_2$ were moved to fit the fibular segments to the arc of the patient's mandible. Next, the angle of the two fibular segments was updated through translation of the connection point $\mathbf{P}_1$. The fibular regions selected for fibular segments in the subview were also changed. Fig. 2(c) shows a three-segment case interactively configured. The two connection points $\mathbf{P}_1$ and $\mathbf{P}_2$ between the segments were similarly translated to fit the contour of the patient's mandible. To maintain the postoperative strength of the reconstructed mandible, the plan was modified under the condition that each fibular segment had sufficient length.

After establishing a surgical plan for all cases, the experimenter computed the proposed three shape indicators: the volume ratio $E_v$, the contour error $E_c$, and the maximum projection $E_p$. Table I shows the computation results based on data for all nine patients in two-segment and three-segment cases. We first confirmed the distribution and the possible outliers of the data using a box plot. On each graph in Fig. 7, the edges of the box represent the 25th and 75th percentiles, the central line is the median, and the whiskers extend to the most extreme values. Next, we conducted a $t$-test hypothesizing normal distribution of the data. The result revealed a significant difference in contour error between the two-segment and the three-segment procedures. The average contour error was 2.78 mm in two-segment cases and 1.64 mm in three-segment cases. This result suggests that three-segment reconstructions are more likely to achieve better reconstruction of the mandibular contour. This result is mathematically reasonable (i.e., linear interpolation of the facial curve). Fig. 7(c) shows the interesting finding that maximum projection $E_p$ values were positive for all nine planning results. The average of the maximum projection $E_p$ assigned by the

dental technician was +1.93 mm. We discussed this finding with the oral surgeon and the dental technician who participated in the experiment, and they agreed with this result. According to their comments, rather than arranging the fibular segments to fit completely within the resection area, they planned it to extend slightly from the patient's native mandible. They made this choice because they felt that better shape can be empirically obtained when the fibular segment protrudes slightly. Our findings demonstrate that the proposed indicators achieve valid quantification that agrees with the empirical knowledge of surgeons and technicians and suggest that empirically established techniques or knowledge in mandibular reconstruction can be confirmed quantitatively through the proposed indicators. We additionally note that over 30 frames per second was achieved during all planning manipulations, and that it was possible to conduct natural, interactive manipulations of the fibular segments superimposed on the volumetrically rendered mandibular images.

### B. Application

Our experiment suggests that mandibular reconstruction using three segments is more likely to produce a mandible matching the original jaw shape than two-segment reconstruction. In spite of this, two-segment reconstruction is still often chosen because of the intraoperative challenges of three-segment procedures. If reconstruction with similar shape and mastication function were possible using two segments rather than three, it would reduce surgery time and would decrease the burden on the surgeon and patient. Because the contour error in lateral cases is relatively smaller than in anterior cases, optimizing the two-segment procedure in preoperative planning is useful to assess various possibilities. We also focused on the finding that better shape can be obtained if the fibular segment protrudes slightly from the original mandible. However, because coordination and placement of fibular segments require complex operation including 3-D translation and rotation in the virtual space, manual adjustment of the reconstruction plans requires a time-consuming process of trial and error.

To address this problem, our second experiment examined how the contour error changes when the fibular segments are locally adjusted, and the possibility of placement to obtain a better result than manual placement by a surgeon using two segments. Based on discussion with the oral surgeon, we have hypothesized an improved surgical procedure: if it were possible to place the fibular segments with greater projection than if they were placed by the surgeon and to trim the projecting portion of the fibular segment, better reconstruction with smaller contour error could be possible using two segments. During surgery, oral surgeons sometimes trim the surface of the cortical bone to adjust the shape, as long as the inner cancellous bone is not exposed. Therefore, in the second experiment, we explored the local position of the connection point $\mathbf{P}_1$ that minimized the contour error under the condition that slight cutting of the projecting portion was allowed. This search was conducted by repositioning the connection point $\mathbf{P}_1$ from –3 to +3 voxels in the *xyz*-direction. Three hundred forty-three placement patterns were examined, and the optimal position with minimum contour error was locally determined. In addition, the following information was used to filter the search results.

1) If the volume ratio $E_v$ after repositioning was less than that in the placement specified by the surgeon, it was removed from the search results.
2) If the maximum projection $E_p$ of the repositioned result was more than +1.93 mm, it was skipped as an invalid placement. The average value obtained by manual placement in the previous experiment was +1.93 mm.

The results of this local search are shown in Table II. In seven of nine cases, better reconstruction with lower contour error $E_c$ was obtained than with manual placement by the surgeon. No position with lower contour error was found for Case 2 or Case 4. The central graph in Fig. 8 shows the average contour error $E_c$ recomputed after repositioning the connection point in the two-segment case. As a reference, the left graph shows the average error of the two-segment cases by manual operation, and the right is the average error of three-segment cases. These graphs demonstrate that the average contour error improved to 2.07 mm from 2.78 mm after the local search around the manually placed connection point. Additionally, in our system, GPU-based parallel computing using CUDA was applied to this search. We have confirmed that average overall computation time to obtain the optimal position was 476.7 ms. This is fast enough in the use of real-time rearrangement to

TABLE II
LOCALLY EXPLORED POSITIONS OF THE CONNECTION POINT $P_1$ THAT MINIMIZES THE CONTOUR ERROR IN TWO-SEGMENT CASES

| Patient | *x* | *y* | *z* [*voxel*] |
|---|---|---|---|
| 1 | 3 | -2 | 1 |
| 2 | 0 | 0 | 0 |
| 3 | -2 | -3 | -1 |
| 4 | 0 | 0 | 0 |
| 5 | 2 | -1 | 1 |
| 6 | -1 | -1 | 0 |
| 7 | 1 | -2 | 3 |
| 8 | -1 | 0 | -1 |
| 9 | 1 | -3 | 1 |

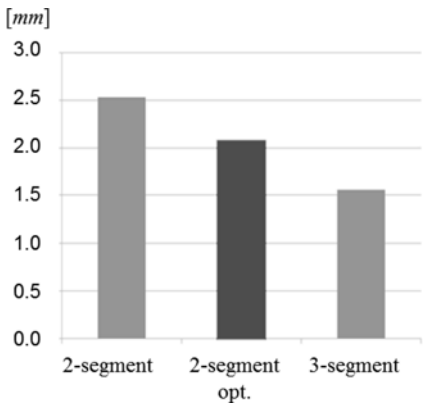


Fig. 8. Contour errors for two-segment, three-segment, and the optimized two-segment case.

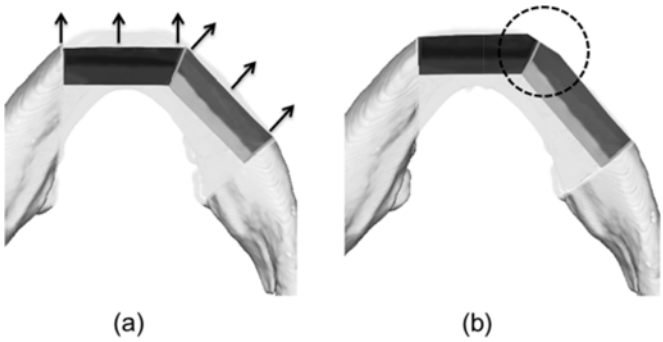


Fig. 9. Local adjustment of the fibular segments to the original mandibular arc under the condition that some cutting of the projecting portion is allowed.

support interactive preoperative planning. This local search suggests the possibility of automatic adjustment of the reconstruction plan, which can reduce the challenges of 3-D adjustment by the users (see Fig. 9). Thus, the shape indicators can quantify the surgical plan from geometrical aspects and improve the applicability of the planning system to optimize mandibular reconstruction. Combining interactive simulation and local exploration of the reconstruction plan based on the shape indicators will provide a good planning environment for fibular transfer surgery.

## V. Discussion

In this paper, we have presented a novel fibular transfer planning system for mandibular reconstruction. Our experiments showed that semiautomatic, interactive planning was achieved by combining direct volume manipulation and real-time local search of placement for fibular segments based on shape indicators. The new system still has the following limitations: 1) The current algorithm for computing the shape indicators can only be applied to the central part of the mandible including the mentum, because the computation results are affected by the scan direction. 2) The effectiveness of the proposed shape indicators was tested in two-segment and three-segment cases. More complex cases, such as a double-barreled reconstruction [9], require further evaluation. 3) GPU-based parallel computing worked in our local optimization of the fibular segments. Efficient optimization algorithms should be implemented to support complex reconstruction cases. We also note that the thinnest region of the cortical bone was about 3.66 mm in our data. Therefore, the filter value of 1.91 mm is considered sufficient to prevent exposure of cancellous bone, suggesting the possibility of further optimization of our system in surgical reconstruction planning. In the future, careful consideration should be given to searching with a maximum threshold projection of approximately 3 or 4 mm. Because the cortical bone of the fibular segment is trimmed, it will also be necessary to analyze postreconstructive strength and the advisability of trimming.

The experiments described in this paper were retrospectively performed using preoperative CT data from previous surgeries. Comparison between virtual planning results and actual postoperative CT volumes is important to confirm the clinical outcomes obtained by optimizing preoperative planning. We are beginning to consider future clinical experiments that will separately address errors in preoperative planning and intraoperative errors from actual surgical procedures. However, to discuss clinical outcomes quantitatively, we should design further long-term experiments, which may include comparison of results obtained with versus without virtual planning. In summary, we plan to investigate the clinical performance of the developed system in our future work.

## VI. Conclusion

This paper presents a new software design for preoperative virtual planning of free fibular transfer in mandibular reconstructive surgery. Direct volume manipulation and visualization of multiple objects allow interactive editing of the surgical plan, including virtual resection, without the need for a surface modeling process. We also introduced three shape indicators, volume ratio, contour error, and maximum projection, to evaluate the surgical plan's geometrical aspects. The proposed indicators quantify the difference between two-segment and three-segment approaches and optimize preoperative planning while satisfying appropriate fibular segment placement margins. Our future work will explore further quantification for physical evaluation of the reconstruction plan, automation of the preoperative planning protocol, and the clinical performance of semiautomatic planning.

## References

[1] A. F. Flemming, M. D. Brough, N. D. Evans, H. R. Grant, M. Harris, D. R. James, M. Lawlor, and I. M. Laws, "Mandibular reconstruction using vascularised fibula," *Brit. J. Plastic Surg.*, vol. 43, no. 4, pp. 403–409, 1990.

[2] R. D. Foster, J. P. Anthony, A. Sharma, and M. A. Pogrel, "Vascularized bone flaps versus nonvascularized bone grafts for mandibular reconstruction: An outcome analysis of primary bony union and endosseous implant success," *Head Neck*, vol. 21, no. 1, pp. 66–71, 1999.

[3] J. P. Shah, "The role of marginal mandibulectomy in the surgical management of oral cancer," *Arch. Otolaryngol. Head Neck Surg.*, vol. 128, pp. 604–605, 2002.

[4] O. Tepper, D. Hirsch, J. Levine, and E. Garfein, "The new age of three-dimensional virtual surgical planning in reconstructive plastic surgery," *Plastic Reconstructive Surg.*, vol. 130, no. 1, pp. 192–194, 2012.

[5] D. L. Hirsch, E. S. Garfein, and A. M. Christensen, "Use of computer-aided design and computer-aided manufacturing to produce orthognathically ideal surgical outcomes: A paradigm shift in head and neck reconstruction," *J. Oral Maxillofacial Surg.*, vol. 67, pp. 2115–2122, 2009.

[6] P. Juergens, Z. Krol, and H. F. Zeilhofer, "Computer simulation and rapid prototyping for the reconstruction of the mandible," *J. Oral Maxillofacial Surg.*, vol. 67, pp. 2167–2170, 2009.

[7] J. Sink, D. Hamlar, D. Kademani, and S. S. Khariwala, "Computer-aided stereolithography for presurgical planning in fibula free tissue reconstruction of the mandible," *J. Reconstructive Microsurg.*, vol. 28, no. 6, pp. 395–403, 2012.

[8] W. H. Wang, J. Y. Deng, M. Li, J. Zhu, and B. Xu, "Preoperative three-dimensional reconstruction in vascularized fibular flap transfer," *J. Craniomaxillofacial Surg.*, vol. 40, pp. 599–603, 2012.

[9] W. H. Wang, J. Zhu, J. Y. Deng, B. Xia, and B. Xu, "Three-dimensional virtual technology in reconstruction of mandibular defect including condyle using double-barrel vascularized fibula flap," *J. Cranio-Maxillo-Facial Surg.*, vol. 41, pp. 417–422, 2013.

[10] Y. Yamanaka, H. Yajima, T. Kirita, H. Shimomura, S. Tamaki, K. Aoki, N. Yamakawa, and Y. Imai, "Mandibular reconstruction with vascularised fibular osteocutaneous flaps using prefabricated stereolithographic mandibular model," *J. Plastic Reconstructive Aesthetic Surg.*, vol. 63, pp. 1751–1753, 2010.

[11] A. K. Antony, W. F. Chen, A. Kolokythas, K. A. Weimer, and M. N. Cohen, "Use of virtual surgery and stereolithography-guided osteotomy for mandibular reconstruction with the free fibula," *Plastic Reconstructive Surg.*, vol. 128, no. 5, pp. 1080–1084, 2011.

[12] G. S. Zheng, Y. X. Su, and G. Q. Liao, "Stereolithographic cutting guide in mandible reconstruction," *Oral Surg. Oral Surg. Oral Med. Oral Pathol. Oral Radiol.*, vol. 113, no. 6, pp. 712–713, 2012.

[13] D. Rohner, R. Guijarro-Martínez, P. Bucher, and B. Hammer, "Importance of patient-specific intraoperative guides in complex maxillofacial reconstruction," *J. Cranio-Maxillo-Facial Surg.*, vol. 41, pp. 382–390, 2013.

[14] S. M. Roser, S. Ramachandra, and H. Blair, "The accuracy of virtual surgical planning in free fibula mandibular reconstruction: Comparison of planned and final results," *J. Oral Maxillofacial Surg.*, vol. 68, pp. 2824–2832, 2010.

[15] Y. Shen, J. Sun, J. Li, T. Ji, M. Li, W. Huang, and M. Hu, "Using computer simulation and stereomodel for accurate mandibular reconstruction with vascularized iliac crest flap," *Oral Surg. Oral Med. Oral Pathol. Oral Radiol.*, vol. 114, no. 2, pp. 175–182, 2012.

[16] B. D. Foley, W. P. Thayer, A. Honeybrook, S. McKenna, and S. Press, "Mandibular reconstruction using computer-aided design and computer-aided manufacturing: An analysis of surgical results," *J. Oral Maxillofacial Surg.*, vol. 71, no. 2, pp. e111–e119, 2013.

[17] J. Kimsal, B. Baack, L. Candelaria, T. Khraishi, and S. Lovald, "Biomechanical analysis of mandibular angle fractures," *J. Oral Maxillofacial Surg.*, vol. 69, no. 12, pp. 1798–1806, 2011.

[18] F. Valente, G. Schiroli, and A. Sbrenna, "Accuracy of computer-aided oral implant surgery: A clinical and radiographic study," *Int. J. Oral Maxillofacial Surg.*, vol. 24, no. 2, pp. 234–242, 2009.

[19] X. Chen, J. Yuan, C. Wang, Y. Huang, and L. Kang, "Modular preoperative planning software for computer-aided oral implantology and the application of a novel stereolithographic template: A pilot study," *Clin. Implant Dent. Relat. Res.*, vol. 12, no. 3, pp. 181–193, 2010.

[20] T. Lee, Y. Sun, Y. Lin, L. Lin, and C. Lee, "Three-dimensional facial model reconstruction and plastic surgery simulation," *IEEE Trans. Inf. Technol. Biomed.*, vol. 3, no. 3, pp. 214–220, Sep. 1999.

[21] A. Bottino, M. De Simone, A. Laurentini, and C. Sforza, "A new 3-D tool for planning plastic surgery," *IEEE Trans. Biom. Eng.*, vol. 59, no. 12, pp. 3439–3449, Dec. 2012.

[22] T. Okada, Y. Iwasaki, T. Koyama, N. Sugano, Y. W. Chen, K. Yonenobu, and Y. Sato, "Computer-assisted preoperative planning for reduction of proximal femoral fracture using 3-D-CT data," *IEEE Trans. Biomed. Eng.*, vol. 56, no. 3, pp. 749–759, Mar. 2008.

[23] M. Levoy, "Efficient ray-tracing of volume data," *ACM Trans. Graph.*, vol. 9, no. 3, pp. 256–261, 1990.

[24] M. Nakao, K. W. C. Hung, S. Yano, K. Yoshimura, and K. Minato, "Adaptive proxy geometry for direct volume manipulation," in *Proc. IEEE Pacific Vis. Symp.*, 2010, pp. 161–178.

[25] K. Imanishi, M. Nakao, M. Kioka, M. Mori, M. Yoshida, T. Takahashi, and K. Minato, "Interactive bone drilling using a 2D pointing device to support microendoscopic discectomy planning," *Int. J. Comput. Assisted Radiol. Surg.*, vol. 5, no. 5, pp. 461–469, 2010.

[26] B. Cabral, N. Cam, and J. Foran, "Accelerated volume rendering and tomographic reconstruction using texture mapping hardware," in *Proc. ACM Symp. Volume Vis.*, 1994, pp. 91–98.

[27] R. Kahler and H. C. Hege, "Texture-based volume rendering of adaptive mesh refinement data," *Visual Comput.*, vol. 16, no. 8, pp. 481–492, 2002.

Authors' photographs and biographies not available at the time of publication.